



#### OPEN ACCESS

##### EDITED BY

Abdoul Aziz Diouf,  
Centre de Suivi Ecologique, Senegal

##### REVIEWED BY

Mehmet Yavuz,  
Artvin Coruh University, Türkiye  
Miluska A. Rosas,  
Pontifical Catholic University of Peru, Peru

##### \*CORRESPONDENCE

Jie Bao,  
✉ jie.bao@pnnl.gov

RECEIVED 14 October 2025  
REVISED 25 February 2026  
ACCEPTED 03 March 2026  
PUBLISHED 23 March 2026

##### CITATION

Bao J, Chen Y, Garayburu-Caruso VA,  
Fluet-Chouinard E, Laan M, Smart J,  
Markham KE, Renteria L, Forbes B,  
Goldman AE and Stegen JC (2026)  
Accuracy evaluation of cost-effective 3D  
reconstruction approaches for  
hydrobiogeochemical processes in non-  
perennial stream riverbeds.  
*Front. Environ. Sci.* 14:1725258.  
doi: 10.3389/fenvs.2026.1725258

##### COPYRIGHT

© 2026 Bao, Chen, Garayburu-Caruso,  
Fluet-Chouinard, Laan, Smart, Markham,  
Renteria, Forbes, Goldman and Stegen.  
This is an open-access article distributed  
under the terms of the [Creative Commons  
Attribution License \(CC BY\)](https://creativecommons.org/licenses/by/4.0/). The use,  
distribution or reproduction in other  
forums is permitted, provided the original  
author(s) and the copyright owner(s) are  
credited and that the original publication  
in this journal is cited, in accordance with  
accepted academic practice. No use,  
distribution or reproduction is permitted  
which does not comply with these terms.

# Accuracy evaluation of cost-effective 3D reconstruction approaches for hydrobiogeochemical processes in non-perennial stream riverbeds

Jie Bao<sup>1\*</sup>, Yunxiang Chen<sup>1</sup>, Vanessa A. Garayburu-Caruso<sup>1</sup>,  
Etienne Fluet-Chouinard<sup>1</sup>, Maggi Laan<sup>1,2</sup>, John Smart<sup>1</sup>,  
Kameron E. Markham<sup>1</sup>, Lupita Renteria<sup>1</sup>, Brienne Forbes<sup>1</sup>,  
Amy E. Goldman<sup>1</sup> and James C. Stegen<sup>1,3</sup>

<sup>1</sup>Pacific Northwest National Laboratory, Riverside, WA, United States, <sup>2</sup>Department of Environmental Sciences, University of California, Riverside, Riverside, CA, United States, <sup>3</sup>Washington State University, School of the Environment, Pullman, WA, United States

Non-perennial streams, characterized by intermittent or episodic flows, comprise over half of global river networks and play an essential role in several ecosystem functions. Accurate stream channel topography is critical for representing flow, hyporheic exchange, and nutrient transport. Although many studies have applied Unmanned Aerial Vehicle (UAV)-based Structure-from-Motion (SfM) to reconstruct river and terrain topography, they have focused more on larger rivers or steep terrain and often relied on RTK-GNSS and ground control points (GCPs), leaving the performance of low-cost workflows for small non-perennial streams lacking evaluations. This study quantitatively evaluates the accuracy of multiple cost-efficient approaches for reconstructing 3-dimensional (3D) stream riverbeds: (1) a UAV imagery-based SfM approach, machine learning-based 3D reconstruction model, (2) Visual Geometry Grounded Deep Structure from Motion (VGGsFm), and (3) Visual Geometry Grounded Transformer for long sequence of images (VGGT-Long), and (4) handheld smartphone LiDAR scanning. The accuracy of the reconstructed topography was assessed against field measurements from a tripod optical level and GCPs GPS positions. UAV-based SfM emerges as the most effective and accessible method for accurately mapping non-perennial streambeds. Its planimetric error is around 1 m, and the ground elevation error is around 0.04 m. Although machine-learning based reconstructions substantially reduce computation time, they do not achieve comparable accuracy. Their planimetric error is over 5 m, and the ground elevation error is above 0.18 m. Likewise, iPhone LiDAR is not suitable for long reaches because cumulative sensor drift degrades positional and vertical precision, compromising the final reconstruction. Propagating these geometric errors into hydraulic and biogeochemical calculations showed that SfM yields relatively modest uncertainty in inferred water depth, velocity, nitrate uptake velocity, and reaeration, whereas the other methods introduce substantially larger

uncertainty. This work exemplifies the significant potential for UAV-based surveys in characterizing stream habitats and conditions and in supporting reliable estimates of hydrobiogeochemical processes.

#### KEYWORDS

error propagation in hydrobiogeochemical processes, handheld smartphone LiDAR scanning, machine learning-based 3D reconstruction model, UAV imagery-based SfM approach, visual geometry grounded deep structure from motion (VGGsFm), visual geometry grounded transformer for long sequence of images (VGGT-long)

## 1 Introduction

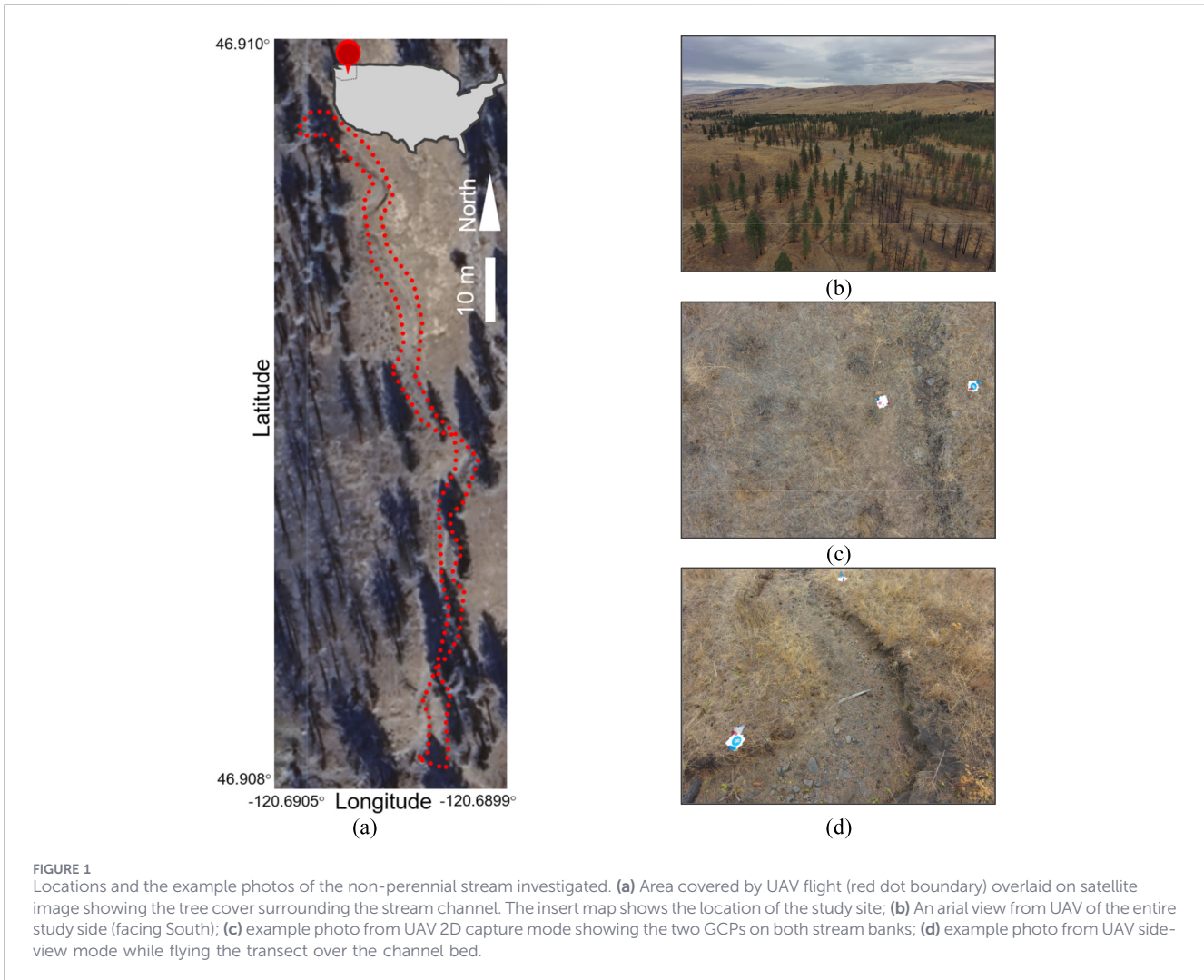
Non-perennial streams, which flow intermittently or episodically, are widespread and constitute over 50% of global river networks (Datry et al., 2014; Snelder et al., 2013; Stegen et al., 2024). Their substantial role to hydrological and biogeochemical connectivity emphasizes the urgency of preserving these systems and to improve our ability to predict and manage the impacts of human activities on water resources (Stegen et al., 2024; Larned et al., 2010). Accurate characterization of stream morphology, including channel geometry and microtopography, is fundamental to understanding and modeling flow routing, sediment transport, nutrient cycling, and habitat formation for aquatic and terrestrial organisms, particularly in simulation-based studies (Entwistle et al., 2018; Benjankar et al., 2018; Legleiter and Harrison, 2018).

Traditionally, riverbed topography is mapped using manual surveying methods involving field equipment like total station theodolite (Keim et al., 1999), terrestrial laser scanner (Lague, 2020), or optical level kit (Guide to optical levels, 2023). While these methods can be highly accurate, they are often time-consuming, labor-intensive, and costly, limiting their use in remote locations, large spatial campaigns, or community science efforts. Advances in photogrammetry and consumer-grade ranging sensors have created lower-cost alternatives that can generate digital elevation models (DEMs) from images or point clouds (Witek et al., 2025; Javernick et al., 2014; Flener et al., 2013; Huai et al., 2025). Among these, Structure-from-Motion (SfM) has become a leading approach because it can recover camera poses and 3D scene structure from overlapping 2D images with high accuracy (Hartley and Zisserman, 2000; Schaffalitzky and Zisserman, 2002; Schönberger and Frahm, 2016; He, 2024; Lindenberger et al., 2021). Camera-equipped unmanned aerial vehicles (UAVs) further improve efficiency by collecting dense imagery over complex terrain with minimal field time (Liu, 2023) for wide range of applications (Eltner et al., 2016; Wang et al., 2025), such as soil erosion (Wang et al., 2025; Medeiros et al., 2025), glacial geomorphology (Sledz et al., 2021; Lamsters et al., 2022), landslide displacements (Chen et al., 2025; Sestras et al., 2025), large-scale riverscape assessment (Giulietti et al., 2022), coastal morphology (Novais et al., 2023). Likewise, LiDAR-equipped UAVs can efficiently provide accurate topographical scans achieving vertical accuracy of  $\pm 5$  cm (Sestras et al., 2025). However, their cost is typically 10 to 100 times higher than that of standard camera-equipped UAVs. In addition, operating these LiDAR-equipped UAVs usually requires highly trained pilots, due to their size and weight. As a result, LiDAR-equipped UAVs are not considered a cost-effective solution for stream reconstruction (Dietrich, 2016).

Substantial pioneering efforts that applied UAV-SfM imagery reconstruction of terrain and stream riverbed topography (Eltner

et al., 2016; Fonstad et al., 2013; Carbonneau and Dietrich, 2017; Dietrich, 2017; Elias et al., 2024; Yavuz and Tufekcioglu, 2023; Dai et al., 2023; Rosas et al., 2023; Clapuyt et al., 2017) demonstrated that utilizing differential Global Navigation Satellite System (GNSS) measurements in real-time kinematic (RTK) or post-processing kinematic (PPK) mode, or calibrating using ground control points (GCPs), reconstructed topography can achieve centimeter-level uncertainty (Eltner et al., 2016; Elias et al., 2024). These advances enable detection and monitoring of small geomorphic changes (Rosas et al., 2023). However, a gap remains between these studies and applications to small non-perennial streams. RTK-equipped UAV surveys often require flying above the tallest site features to meet safety and operational constraints. In small, tree-lined non-perennial streams, canopy cover and tight channel corridors can limit visibility and restrict flight paths, making low-altitude, under-canopy imaging with lightweight, simple camera-equipped UAVs more feasible than standard RTK-based approaches. However, studies evaluating SfM accuracy for small non-perennial streambed topography using recreation-grade UAVs remain limited.

Although SfM is a long-standing, top-performing approach for topographic reconstruction, it is often computationally expensive for large image collections. Recent research has therefore explored deep-learning approaches, such as Ba-net (Tang and Tan, 2018), Deepv2d (Teed and Deng, 2018), and Droid-slam (Teed and Deng, 2021), that replace or augment standard SfM. By training on large datasets of images, camera poses, and 3D scenes, these methods aim to enable faster inference while maintaining competitive accuracy on new imagery (Wang et al., 2023; Deng et al., 2025; Wang et al., 2022). In parallel, consumer devices now integrate active depth sensing. LiDAR-equipped smartphones, such as recent iPhone models, offer portable tools for near-real-time mapping and may help democratize high-precision surveying for individuals and community science groups. iPhone LiDAR used with apps such as Polycam (2023), Scaniverse (2023), SiteScape (2024), SRL (2024), etc. uses laser pulses to measure distances and generate detailed 3D maps of surrounding surfaces. LiDAR sensors are still uncommon on Android devices, so comparable built-in capabilities are limited. In geoscience and environmental applications, iPhone LiDAR typically achieves errors ranging from centimeters to tens of centimeters, depending on the scan area (Krauskova et al., 2025; Oikawa et al., 2025; Luetzenburg et al., 2021; Tatsumi et al., 2022; Gollob et al., 2021; Mokros et al., 2021). However, these devices rely on internal positioning and orientation systems that can introduce drift and cumulative errors—especially when scanning elongated features such as stream channels—which may lead to meter-level positioning errors (Krauskova et al., 2025). Thus, the accuracy of iPhone LiDAR for reconstructing small non-perennial streambeds also requires quantitative evaluation.



A major motivation for reconstructing streambeds using the approaches above is hydrobiogeochemical process modeling. Prior work has demonstrated strong sensitivity of flow simulations to DEM quality. For example, Hardy et al. (1999) showed that small DEM differences caused by resolution changes can lead to nearly 100% differences in discharge estimates. Cook and Merwade (2009) similarly showed that differences in DEM accuracy can produce more than 25% differences in predicted inundation maps. Dietrich (Dietrich, 2016) compared discharge differences using SfM-versus LiDAR-reconstructed streambeds. In addition, previous studies (Kurz et al., 2017; Young and Huryn, 1999; Tromboni et al., 2022; Mulholland et al., 2008; Bernhardt et al., 2018) have shown that, besides incident light, stream biogeochemical processes are most strongly related to surface-water velocity and depth; therefore, uncertainty in surface-flow estimation directly affects biogeochemical process modeling. However, most prior research has focused on large-scale or synthetic river channels and reaches, so the impacts of reconstruction errors and uncertainties for small non-perennial streambeds on associated hydrobiogeochemical process estimates remain unclear.

This study addresses these gaps by benchmarking cost-effective approaches for reconstructing non-perennial streambed topography against ground truth from tripod optical leveling kit measurements

and GCP GPS positions. The GCPs are used solely to evaluate reconstruction accuracy and are not used for calibration. We evaluate four competing methods: (1) a UAV imagery-based SfM approach, (2) VGGsFm, (3) VGGT-Long, and (4) handheld smartphone LiDAR scanning. For each method, we quantify planimetric and ground-elevation errors between reconstructed surfaces and ground truth, and we further assess how these geometric errors propagate into hydrobiogeochemical modeling outcomes, including water depth, velocity, nitrate uptake velocity, and reaeration rates. Section 2 introduces the four reconstruction approaches and the error propagation evaluation method, Section 3 presents the comparative results, and Section 4, 5 discuss implications and conclude the study.

## 2 Methodology

### 2.1 Study domain and data collection

The stream investigated in this study is a section of Umtanum Creek in Washington state USA, located at latitude 46°54'34.2"N and longitude 120°41'24.4"W (Figure 1a). Umtanum Creek drains a

small, mixed land-use basin characterized by a mediterranean climate (wet winters, dry summers), episodic high flows, and extended low-flow and dry periods, making it representative of non-perennial streams found widely across the interior Pacific Northwest and other semi-arid regions of western North America. The surrounding landscape consists primarily of shrub-steppe and grassland with ~10% ponderosa pine, as the aerial view shown in Figure 1b. Data collection was conducted on 18 October 2024, during which the non-perennial stream was completely dry.

Ground truth measurements of the stream riverbed were obtained using a tripod-mounted optical level kit (BOSCH GOL 32CK 32X). Eighteen transects were evenly distributed along a ~200-m-long section of the stream, spaced approximately 10 m apart. Each transect has two GCPs, one on the left bank (facing downstream) and one on the right. Along each transect, 7–8 points were measured at average intervals of 60 cm. The position of the tripod optical level kit served as the reference point, and two tripod positions were used both approximately ~150 m from the stream. The relative height differences between the points on the transects and this reference point were recorded, and then be used to back calculate the absolute elevation of the points along transects (King, 2024).

For the reconstruction, images were collected using the UAV Skydio 2 (Skydio, 2024). The UAV was programmed to firstly use 2D capture mode that sets the camera facing the ground at 90° (Figure 1c), a flight height of 6.5 feet (~2 m), and an overlap of 80% between two adjacent photos. An example of the photos in 2D capture mode is shown in Figure 1c. After the 2D capture mode, the UAV flew along the boundary of the survey region in side-view mode, in which the camera tilted 60° downward from horizontal (Figure 1d). A total of 3,098 photos were captured for the investigated stream. Likewise, for the iPhone LiDAR scanning, one field staff member held an iPhone and walked along the centerline of the dry streambed from the downstream to the upstream end. During scanning, the 3D Scanner app displayed, in real time, which regions had been adequately captured and which had not. The field staff member adjusted the iPhone's orientation to target areas flagged as missing data and repeated this procedure until the app indicated full coverage. The app then processed the collected data and generated a 3D model of the streambed in a few minutes.

## 2.2 Reconstruction of riverbed

Four approaches were evaluated for reconstructing the riverbed of the investigated non-perennial stream. The first one is the standard Structure from Motion (SfM) (Ullman, 1979) algorithm to transform the collected UAV images into 3D representations of ground surface. The second one is a machine learning based approach, Visual Geometry Grounded Deep Structure from Motion (VGGsFm) (Wang et al., 2023) using the same UAV images. The third one is Visual Geometry Grounded Transformer for long sequence of images (VGGT-long) (Deng et al., 2025) using the same UAV images as well. The fourth approach is 3D scanning using the Apple iPhone integrated LiDAR (Shan and Toth, 2018). The first three methods are based on the same UAV imagery, while the fourth provides a distance point cloud directly measured by laser pulses. Because the horizontal origins differed across reconstructions, each reconstructed riverbed was translated in x and y directions so that the 11th GCP on the left

bank coincided with its GPS measured position. The machine-learning reconstructions (VGGsFm and VGGT-Long) lacked absolute elevation referencing. Their surfaces were therefore vertically offset by +833 m and +828 m, respectively, so that the elevation at GCP-L #11 matched the ground-truth measurement. In contrast, the SfM and iPhone LiDAR reconstructions used sensor-derived elevations referenced to sea level and required no vertical adjustment.

### 2.2.1 Structure from motion algorithm

The standard SfM algorithm that reconstructed the riverbed from UAV photos was implemented in OpenDroneMap (ODM) (Open Drone Map, 2025). The SfM process initiates with the detection of distinctive feature points in the images. Scale-Invariant Feature Transform (SIFT) (Lowe, 1999; Gonzalez and Woods, 2017) is one of the most popular methods that detect the distinctive feature points from each image and match them across multiple images. The GPS and elevation information in the image EXIF (IPTC, 2025) are usually used to determine the query image candidates in a feature matching step to accelerate the calculation. After the feature points detection and matching for all the images, all the matched points' coordinates can be expressed as  $\vec{x}_{f,i}$ , where the subscript  $i$  refers to the index of matching points on the image frame  $f$ . The two-view geometry method estimates the essential matrix  $E$  for enforcing  $\vec{x}_{f_0,i}^T E \vec{x}_{f_0+1,i} = 0$ , where  $\vec{x}_{f_0,i}$  and  $\vec{x}_{f_0+1,i}$  stand for the coordinate matrix of the matching points on the frames  $f_0$  and  $f_0 + 1$ . The essential matrix  $E$  then can be decomposed as  $E = tR$  by the Singular value decomposition (SVD) method, where  $t$  covers the camera translation matrix, and  $R$  covers the camera rotation matrix. The 3D world coordinates of the matching feature points in the first two picked images can be calculated by the linear triangulation algorithm. After initialization of the 3D scene from the firstly picked images, new images can be added into the reconstruction one by one. This step can be repeated until all the images and feature points are added into the reconstructed 3D scene. When reprojecting the 3D scene points back to each image using their own camera translation and rotation matrixes, there are unavoidable errors. For reducing these reprojection errors, SfM conducts global optimization to adjust or fine tune all the camera project matrixes and the 3D scene points through Bundle Adjustment (BA) (Triggs et al., 1999; Lourakis and Argyros, 2009). The algorithm then performs dense reconstruction using advanced Multi-View Stereo (MVS) techniques, projecting all the pixels, no matter if feature points or not, on each image to the 3D scene using the global optimized camera projection matrixes. The dense point cloud then is processed into a 3D mesh, with texturing algorithms mapping the original images onto the mesh to produce a photorealistic model. Finally, ODM generates high-resolution Digital Elevation Models (DEMs), isolating the ground surface, and orthophotos, which are geometrically corrected aerial images with uniform scale, producing accurate and detailed geospatial data.

### 2.2.2 Visual geometry grounded deep structure from motion

Recent deep learning methods aim to enhance or replace the standard SfM method. VGGsFm is the first fully differentiable

pipeline, so it can be trained in an end-to-end manner and once achieved state-of-the-art accuracy in 2023. It demonstrated that learned systems can surpass classic SfM on real-world dataset such as buildings and street scenes (Wang et al., 2023). VGGsFm implements SfM via a single function  $f_{\theta}(I) = P, X$ . The input  $I$  represents all the images. The output  $P$  represents the camera parameters, and  $X$  represents the point cloud of the reconstructed 3D scene. All the parameters  $\theta$  in function  $f_{\theta}$  is trainable by minimizing the training loss  $L$ . The loss is the differences between the function outputs ( $P, X$ ) and the ground truth camera parameters and scene. The training dataset for the ground truth is usually from either standard SfM or the synthetic 3D scenes. The reconstruction function  $f_{\theta}$  is decomposed into four seamless stages: 1) point tracker  $T = \tau(I)$ ; 2) initial camera estimator  $\hat{P} = \zeta_P(I, T)$ ; 3) triangulator  $\hat{X} = \zeta_X(T, \hat{P})$ ; and 4) Bundle Adjustment  $P, X = BA(T, \hat{P}, \hat{X})$ . The point tracker uses 2D convolutional architecture (Harley et al., 2022; Karaev et al., 2023) as the backbone. The initial camera estimator uses ResNet (He et al., 2016) as the backbone. The triangulator uses transformer model (Dosovitskiy, 2024; Vaswani et al., 2017). The Bundle Adjustment uses fully differentiable second-order Theseus solver (Pineda, 2023). In this study, the publicly available pre-trained model was directly applied on the UAV images to reconstruct the stream riverbed. The pre-trained model was trained by MegaDepth (Li and Snavely, 2018) and three additional datasets published by Lin et al. (2024), Zhang et al. (2022), Wang et al. (2024).

### 2.2.3 Visual geometry grounded transformer for long sequence of images

VGGT is a feed-forward neural network that performs 3D reconstruction from one, a few, or hundreds of input views of a scene. VGGT moved one step further from VGGsFm. It does not separate the reconstruction into multiple stages. Instead, it uses one standard large transformer model (Dosovitskiy, 2024; Vaswani et al., 2017), with no particular 3D or other inductive biases, but trained on a large number of publicly available datasets with 3D annotations. The detailed list of the training datasets is available in Wang et al. (2022). The model inputs are the images, and the outputs are camera parameters, images' depth map, point cloud, and point tracks. The original VGGT model obtained a new state-of-the-art in reconstruction quality in early 2025, but the limitation is significant computational and memory cost, which restricts the applications to short image sequences (Deng et al., 2025). A new framework, based on VGGT, was proposed and demonstrated by Deng et al. (2025) for long image sequences, named as VGGT-Long. It processes long sequences by dividing them into smaller chunks, thereby handling the input image stream in a sliding window manner. For extending VGGT to long-sequence image datasets, it utilizes VGGT's point map to perform lightweight loop closure and alignment on the output chunks. VGGT-Long achieved state-of-the-art accuracy for the long sequence dataset (Geiger et al., 2012; Sun et al., 2020; Gaidon et al., 2016) in mid-2025, without requiring model retraining. In this study, the VGGT-Long framework with the pre-trained VGGT model was directly applied on the UAV images to reconstruct the stream riverbed.

### 2.2.4 Smart phone integrated LiDAR

An integrated LiDAR on Apple iPhone 15 Pro Max was used to scan the stream riverbed. LiDAR enables advanced 3D scene reconstruction by emitting laser pulses and measuring the time it takes for the light to bounce back after hitting an object. This process generates depth data that precisely maps the environment. By combining LiDAR depth with RGB camera imagery and the phone's motion sensors, the device reconstructs 3D geometry in real time using an RGB-D pipeline based on Simultaneous Localization and Mapping (SLAM) (Jaulin, 2011; Magnabosco and Breckon, 2013). The phone estimates its 6 degrees of freedom (6-DoF) pose via visual-inertial odometry that fuses camera tracking with the accelerometer and gyroscope (Comport et al., 2010), while LiDAR depth frames are filtered and back-projected to 3D points, then transformed into the world frame coordinates. Successive depth observations are aligned to the growing model and fused into a global surface representation, commonly using volumetric integration such as a truncated signed distance function (TSDF) with weighted updates (Li et al., 2024; Perera et al., 2015). A triangle mesh is then extracted (e.g., Marching Cubes (Lorenson and Cline, 1987)) and optionally smoothed/decimated and textured by projecting RGB frames onto the mesh. The implementation of the algorithms and the associated hardware in the iPhone are accessible in Apple ARKit (Apple, 2024). In this study, the scanning and reconstruction were implemented in the fully integrated App, 3D Scanner (SRL, 2024). This iPhone integrated LiDAR was used for evaluating the accuracy of a cost-effective alternative in the application of stream riverbed reconstruction.

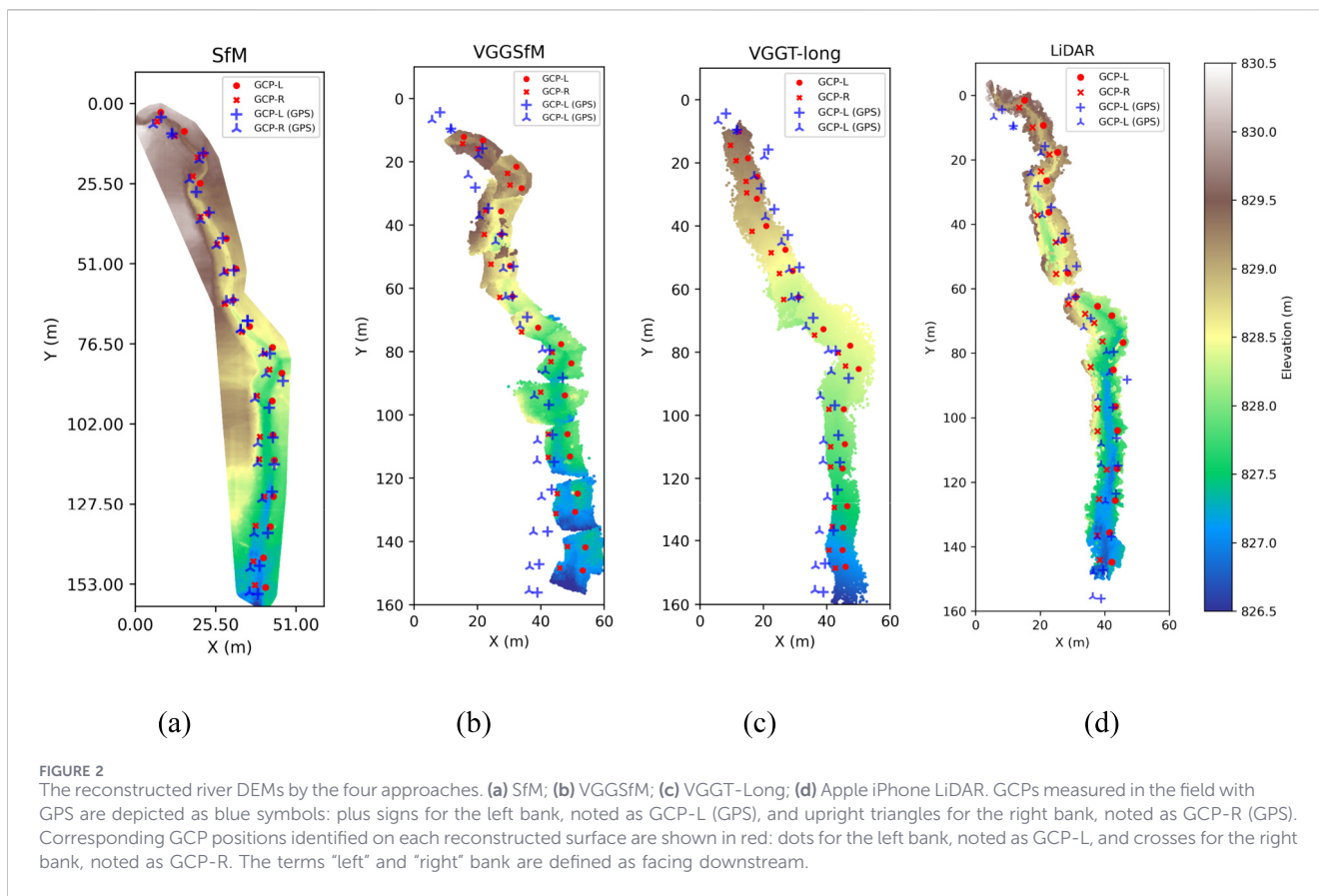
## 2.3 Error propagation in hydrobiogeochemical processes modeling

River hydrobiogeochemical processes at the reach scale are strongly linked to river topography (Shogren et al., 2019; Li et al., 2015). Consequently, the accuracy of reconstructed streambed topography directly affects the reliability of studies on hydrodynamic analyses. Thus, estimation of biogeochemical processes are only as reliable as the underlying estimates of water depth and velocity (Harvey et al., 2024; Appling et al., 2018), which in turn depend on the accuracy of the reconstructed streambed.

In this study, Manning's equation was utilized to estimate the water depth and velocity of open-channels by converting each reconstructed cross-section into its nearest trapezoidal shape and determining the channel slope between successive cross-sections (Manning, 1891; Gioia and Bombardelli, 2001). The flow rate in an open-channel can be calculated using the following method:

$$Q = \frac{1}{n} AR^{2/3} S_0^{1/2} \quad (1)$$

where  $Q$  is flow rate ( $m^3/s$ ),  $n$  is Manning roughness, which is  $\sim 0.03$  for natural channel with stones and weeds.  $A = bH + zH^2$  is wetted cross section area, where  $b$  is the bottom width,  $H$  is water depth, and  $z$  is side slope.  $R = A/(b + 2H\sqrt{1 + z^2})$  is hydraulic radius.  $S_0$  is streambed slope. With given flow rate and the fitted trapezoid cross section, the water depth can be solved by the



bisection iteration method from Equation 1, and subsequently water velocity can be calculated.

After having the estimated water depth and velocity, the streambed nitrate uptake velocity ( $u_f$ ) can be estimated by Grant et al. (2018):

$$u_f = 0.17u_\tau \left( \frac{\nu}{D_m} \right)^{-2/3} c_1 [NO_3^-]^{c_2} \quad (2)$$

where  $\nu = 1 \times 10^{-6} \text{ m}^2/\text{s}$  is water viscosity,  $D_m = 1.7 \times 10^{-9} \text{ m}^2/\text{s}$  is nitrate molecular diffusion in water (Piciooreanu et al., 1997),  $c_1 = 0.0032$ , and  $c_2 = -0.49$  (Grant et al., 2018).  $[NO_3^-]$  is nitrate concentration. In the Yakima River Basin, our field survey in 2021 shows that the nitrate concentration varies between 0.0005 and 0.1, with mean of 0.008 mol/m<sup>3</sup> (Grieger, 2014). In this study, 0.008 mol/m<sup>3</sup> is used for estimating  $u_f$ .  $u_\tau$  is shear velocity, and can be estimated by Ferguson (2007), Ferguson (2022):

$$u_\tau = \frac{U \sqrt{c_3^2 + c_4^2 (H/D_{84})^{5/3}}}{c_3 c_4 H / D_{84}} \quad (3)$$

where  $U$  is flow velocity,  $D_{84}$  is 84th percentile of grain size distribution, which is ~0.13 m. The constants  $c_3 = 6.5$  and  $c_4 = 2.5$  (Ferguson, 2022).

The reaeration can be estimated by Owens' velocity-depth formula  $k_0 = 5.32U^{0.67}H^{-1.85}$  (Owens et al., 1964), which is usually applied for the stream  $0.1 \text{ m} < H < 3 \text{ m}$  and  $0.03 \text{ m/s} < U < 1.5 \text{ m/s}$ . The water depth and velocity in the investigated stream are partially in this range by the estimation approaches introduced above.

Relative error distributions for the reconstructed streambed from different approaches were computed by comparison with estimates derived from the ground-truth cross sections measured with the tripod optical level kit. Results for the flow rates between 0.01 and 3 m<sup>3</sup>/s were used to estimate the errors at different flow conditions for the small non-perennial stream.

### 3 Results

#### 3.1 Reconstruction geometric errors

The reconstructed DEMs obtained using the four approaches are displayed in Figures 2a–d. Upstream lies to the north ( $Y = 0$ ). Ground elevation is referenced to sea level (North American Vertical Datum of 1988), based on measurements obtained from the pressure sensor mounted on the UAV. GCPs measured in the field with GPS and the ones identified on each reconstructed surface are shown in Figure 2. The terms "left" and "right" bank are defined as facing downstream. GCPs are numbered sequentially from south to north, ranging from 1 to 18.

As visible in Figure 2, the GCPs from SfM reconstructed riverbed are very close to the GPS measurements, whereas VGGSfM, VGGT-Long, and iPhone LiDAR exhibit larger misalignments, implying substantial river distortions in those reconstructions. To quantify the accuracy of these methods, the distance between the ground truth GCP locations and the ones from

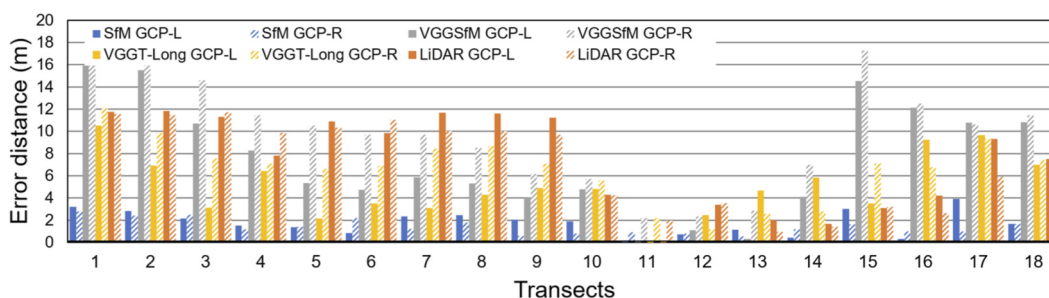


**FIGURE 3** Error distances between the GCP locations from the reconstructed riverbed and the ground truth locations derived from GPS information. Transect numbers increase from downstream to upstream. GCP-L represents the GCP on the left stream bank, and GCP-R represents the GCP on the right bank. The terms “left” and “right” bank are defined as facing downstream.

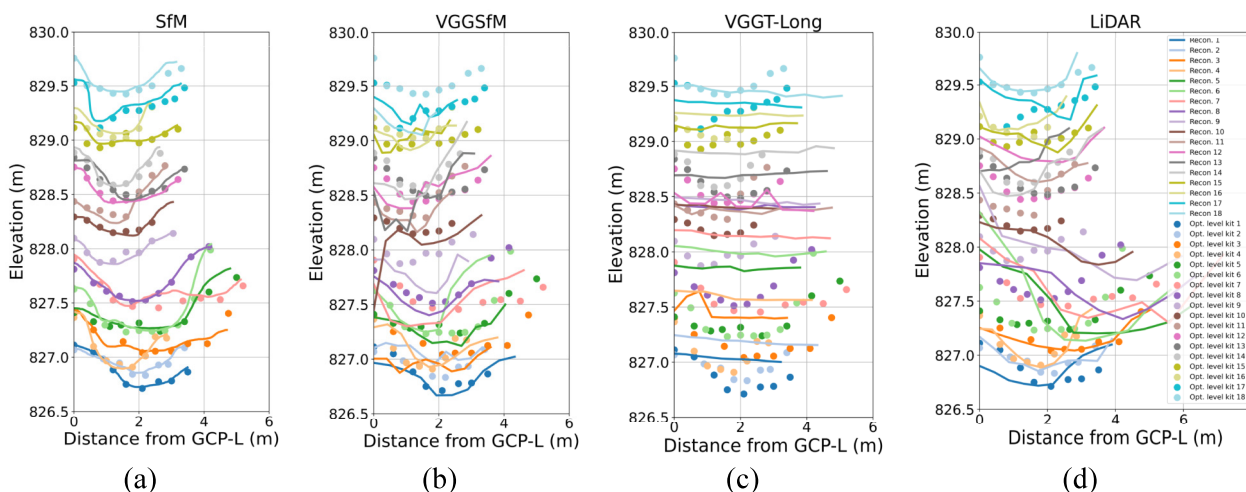


**FIGURE 4** Comparison between the reconstructed riverbed and the on-site optical level kit measurements at the 18 transects for the four reconstruction approaches. (a) SfM; (b) VGGsFm; (c) VGGT-Long; (d) Apple iPhone LiDAR. The dots represent the field-measured elevations obtained using a tripod optical level kit (BOSCH GOL 32CK 32X). The solid lines represent the corresponding transects extracted from the reconstructed riverbeds.

the reconstructed surfaces were calculated for each GCP as shown in Figure 3. The mean error distance for the SfM reconstructed riverbed is around 1.59 m for all the 36 GCPs (left and right banks at 18 transects), with standard deviation of the mean error distance 0.9 m. Note that consumer-grade GPS typically achieves 1–5 m accuracy in open-sky conditions (NOAA, 2025), so a mean error of 1.59 m is within the expected GPS uncertainty. The other three approaches produced substantially larger errors, with mean error distances of 8.71 m (VGGsFm), 5.87 m (VGGT-Long), and 7.26 m (iPhone LiDAR), with the standard deviation of error distance 5.1, 2.8, and 4.0 m respectively.

Comparisons between reconstructed cross sections and field-measured elevations for the 18 transects are shown in Figures 4a–d. The results indicate that the standard SfM approach provided highly accurate reconstructions, aligning very well with the field-measured data across all 18 transects. Although VGGsFm and iPhone LiDAR partially captured the general topographic features of the 18 transects, they deviated marginally from the overall slope of the stream. VGGT-Long, on the other hand, failed to capture the

correct topography of the riverbed, as its reconstructed riverbed exhibited no concave shape characteristic of the actual river.

For the standard SfM, the RMSE (Figure 5a) across all 18 transects was less than 0.1 m, and the average RMSE was 0.04 m for these transects, with standard deviation of RMSE 0.02 m. The mean error (Figure 5b) for the standard SfM method across all transects ranged up to 0.05 m, with an average of 0.02 m and standard deviation of 0.03 m. In the case of VGGsFm, the RMSE for the 18 transects mostly lay between 0.1 m and 0.4 m, with an average RMSE of 0.18 m and standard deviation of 0.09 m. The mean error for VGGsFm ranged up to 0.2 m, with an average mean error of -0.08 m and standard deviation of 0.12 m. For VGGT-Long, the RMSE values for the transects predominantly ranged from 0.1 m to 0.7 m, with an average RMSE of 0.31 m and standard deviation of 0.2 m. The mean error for VGGT-Long spanned from -0.1 m to 0.7 m, with an average mean error of 0.24 m and standard deviation of 0.24 m. Lastly, the iPhone LiDAR produced RMSE values for the transects mainly between 0.1 m and 0.5 m, with an average RMSE of 0.2 m and standard deviation of

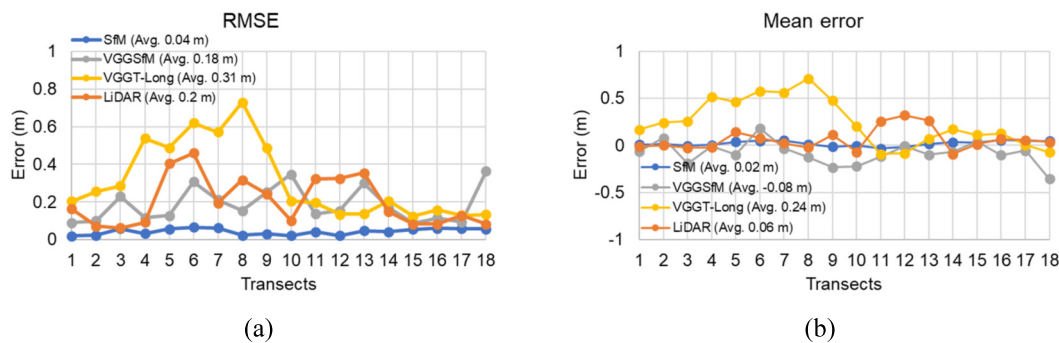


FIGURE 5 Error indices: (a) the RMSE and (b) the mean error of each transect for the four reconstruction approaches. The averaged errors of the 18 transects are listed in the legends respectively.

0.13 m. Its mean error ranged between  $-0.1$  m and  $0.4$  m, with an average mean error of  $-0.06$  m and standard deviation of  $0.11$  m.

### 3.2 Estimation of error propagation in hydrobiogeochemical modeling

Results for flow rates between  $0.01$  and  $3 \text{ m}^3/\text{s}$  are shown in Figure 6. For the SfM-reconstructed streambed, relative errors in estimated water depth and velocity were within  $\pm 10\%$ , with interquartile ranges (IQRs) below  $\pm 5\%$ . In contrast, geometric errors in the VGGsM reconstruction produced water-depth errors up to  $\pm 30\%$  and velocity errors from  $-50\%$  to  $+10\%$ . These errors were slightly larger at low flow rates ( $0.01\text{--}0.5 \text{ m}^3/\text{s}$ ) and decreased as discharge increased. For VGGT-Long, geometric error resulted in water-depth errors from  $-10\%$  to  $+40\%$  and velocity errors within  $\pm 20\%$ . For iPhone LiDAR, water-depth errors ranged from  $-15\%$  to  $+25\%$ , and velocity errors were within  $\pm 20\%$ .

These errors in water depth and velocity propagated to the estimated nitrate uptake velocity and reaeration rate constant by the approaches introduced in Section 2.2.5. For SfM, relative errors in both nitrate uptake velocity and reaeration rate constant were within  $\pm 20\%$ , with IQRs below  $\pm 10\%$ ; errors decreased slightly with increasing flow rate. For VGGsM, nitrate uptake velocity errors ranged from  $-40\%$  to  $+5\%$ , while reaeration rate constant errors were within  $\pm 50\%$ . For VGGT-Long, nitrate uptake velocity errors ranged from  $-30\%$  to  $+10\%$  (with IQRs generally below  $\pm 10\%$ ), and reaeration rate constant errors ranged from  $-40\%$  to  $+10\%$ . For iPhone LiDAR, nitrate uptake velocity errors ranged from  $-35\%$  to  $+10\%$ , and reaeration rate constant errors ranged from  $-40\%$  to  $+10\%$ .

Young and Huryn (1999) reported that metabolism metrics, gross primary production (GPP), production-to-respiration ratio (P/R), and net ecosystem metabolism (NEM), are strongly related to water depth and velocity in perennial streams. Therefore, relative errors in modeled metabolism for these parameters may be comparable to the error distributions observed for water depth and velocity (Figures 6a,b). However, quantitative metabolism modeling for non-perennial streams remains limited, and robust characterization of error propagation in such systems requires further study.

## 4 Discussion

### 4.1 Practical feasibility of low-cost streambed reconstruction

This study evaluated cost-effective methods for reconstructing the stream bed topography of a non-perennial stream. Although our analysis is based on a single reach in Umtnum Creek, its hydroclimatic setting (semi-arid, Mediterranean-type precipitation), small channel dimensions, shallow water depths, and intermittent flow regime are characteristic of many non-perennial streams in the interior western United States and other dryland regions (Gellenbeck, 1999; Mundorff et al., 1977). Therefore, our findings on reconstruction accuracy and error propagation are likely transferable to similar systems, while recognizing that performance may vary with channel complexity, substrate, vegetation cover, and lighting conditions.

From an implementation perspective, conventional field surveying required substantially more time and personnel than the low-cost sensing approaches. Acquiring optical level measurements for 18 transects and GPS positions for GCPs took  $\sim 6$  h with four staff (we recommend  $\geq 3$  people to maintain efficiency and reduce recording errors). In comparison, UAV image acquisition required  $\sim 1.5$  h with two operators (primarily for institutional safety compliance; a single operator would likely achieve similar efficiency), and iPhone LiDAR scanning required  $\sim 20$  min. Processing time varied by method: SfM required  $\sim 16$  h on a CPU workstation (Intel Xeon W7-2495X), whereas inference using pre-trained learning-based models required  $\sim 30$  min on a high-end GPU (NVIDIA H100), though CPU-only runs can take several hours. iPhone LiDAR reconstruction took  $\sim 10$  min directly on the device. Overall, these comparisons indicate that low-cost reconstruction approaches can substantially reduce field labor and associated costs relative to conventional surveying, even if they shift part of the effort to computation during post-processing.

### 4.2 Comparative accuracy of reconstruction methods

UAV-SfM has been widely applied to reconstruct terrain and riverbed topography, with multiple studies reporting centimeter-

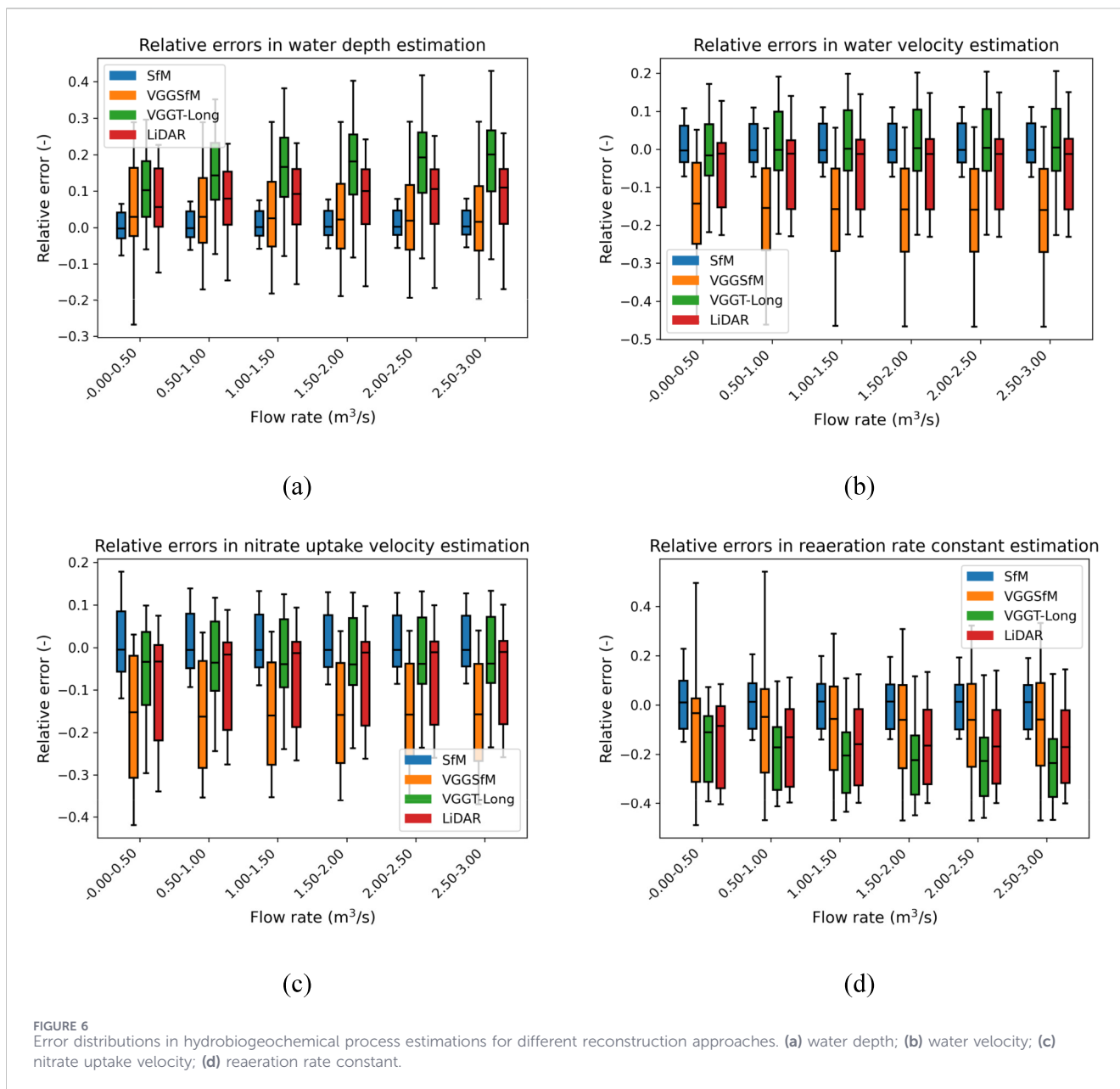


FIGURE 6 Error distributions in hydrobiogeochemical process estimations for different reconstruction approaches. (a) water depth; (b) water velocity; (c) nitrate uptake velocity; (d) reaeration rate constant.

level accuracy (Eltner et al., 2016; Fonstad et al., 2013; Carbonneau and Dietrich, 2017; Dietrich, 2017; Elias et al., 2024; Yavuz and Tufekcioglu, 2023; Dai et al., 2023; Rosas et al., 2023; Clapuyt et al., 2017). However, many high-accuracy workflows rely on RTK/PPK-equipped UAVs and/or GCPs to constrain camera poses and georeferencing (Eltner et al., 2016; Elias et al., 2024). These requirements can be difficult to meet in small, tree-lined non-perennial streams. Operationally, RTK-equipped UAV surveys often require flying above the tallest site features to satisfy safety and flight constraints (DJI Matrice 300 RTK user manual, 2025). In narrow riparian corridors, canopy cover and trunks can obstruct imagery and restrict flight paths, making low-altitude, under-canopy flights with lightweight, maneuverable RGB camera UAVs more feasible than standard RTK-based survey configurations. Low-altitude flights are also advantageous because reconstruction error generally increases with sensor-to-surface distance

(i.e., flight height) (Eltner et al., 2016). Together, these constraints motivate evaluating whether SfM can still provide accurate streambed topography in settings where RTK/PPK motion data and GCP calibration are unavailable for reconstruction of small non-perennial stream.

For the investigated stream in this study, the SfM reconstruction achieved centimeter-level cross-sectional accuracy (RMSE = 4 cm; mean error = 2 cm) and ~0.5% relative planimetric error without relying on RTK/PPK positioning or calibrations with GCPs. This performance likely benefited from the low flight height (~2 m), consistent with prior findings that reconstruction error increases with sensor-to-surface distance (Eltner et al., 2016). While UAVs typically do not fly at such low altitudes for geoscience surveys in prior studies (Eltner et al., 2016; Frankl et al., 2015) reported SfM errors of 1.7–19 cm using a handheld camera at ~2 m standoff distance. Together, these results indicate that lightweight,

recreation-grade UAVs can provide reliable reconstructions of small non-perennial streambeds when low-altitude flights beneath the canopy are feasible.

In contrast, the machine-learning methods (VGGsFm and VGGT-Long) exhibited substantial planimetric errors, with mean horizontal GCP offsets of 8.71 m and 5.87 m, respectively, and transect RMSEs averaging 0.18 m (VGGsFm) and 0.31 m (VGGT-Long). For shallow streams with depths typically less than 1 m, which is a common condition for non-perennial streams (Stegen et al., 2024), vertical errors of this magnitude, combined with meter-scale planform misplacement, are too large to yield dependable topographic information. Benchmark results for VGGT-Long reported in its original application (Deng et al., 2025) similarly indicate meter-level errors in large-scale outdoor scenes, underscoring its limitations in capturing complex, fine-scale streambed morphology. Moreover, the performance of learning-based models depends strongly on the training data (Wang et al., 2023; Wang et al., 2022). The public datasets used to pre-train VGGsFm and VGGT-Long are dominated by human-made objects and urban street scenes, with natural, undeveloped environments underrepresented (Li and Snively, 2018; Lin et al., 2024; Zhang et al., 2022; Wang et al., 2024). This domain mismatch likely contributed to the models' underperformance in this study and may be remediated by inclusion of more natural stream channel-like data in the pre-training.

Reconstruction from iPhone LiDAR was also insufficiently accurate for purposes of modeling streambed functions, with a mean horizontal GCP error of 7.26 m and an average transect RMSE of 0.20 m. This limitation arises from the inherent reliance of iPhone LiDAR on positional information derived from internal phone sensors, including the gyroscope, accelerometer, and pressure sensor (Krauskova et al., 2025). As the iPhone is moved along the streambed during the scanning process, drift accumulates, producing progressively larger georeferencing and elevation errors over distance. This behavior is consistent with Krauskova et al. (2025), who mapped a ~160 m stream reach and observed rapidly increasing positional and elevation errors beyond ~60 m, reaching ~2 m positional error and ~0.2 m elevation deviation by 160 m. Prior works similarly suggest iPhone LiDAR is most suitable for short scans (e.g., ~20 m, or up to ~60 m with ~20 cm error) (Krauskova et al., 2025; Liang et al., 2018a; Liang et al., 2018b). Accuracy can further degrade under dense vegetation (Krauskova et al., 2025; Moudrý et al., 2019), which likely contributed in this investigated streambed because portions of the bed were obscured by 20–50 cm tall dry grass.

### 4.3 Propagation of errors to hydraulic and biogeochemical estimates

Linking geometric reconstruction error to hydrobiogeochemical inference, we further showed that topographic inaccuracies propagate directly into estimated water depth, velocity, nitrate uptake velocity, and reaeration rate constant. This is expected because environmental responses to topographic inputs are often nonlinear: small elevation errors can alter wetted area, hydraulic radius, and local slope, producing comparatively large changes in modeled flow fields (Dietrich, 2016; Hardy et al., 1999; Cook and Merwade, 2009).

As detailed in Section 3.2, the SfM-based reconstruction produced the lowest velocity error ( $\pm 10\%$ ). iPhone LiDAR and VGGT-Long reconstructions produced similar velocity errors (both  $\sim \pm 20\%$ ), whereas VGGsFm reconstruction produced the largest velocity errors ( $-50\%$  to  $+10\%$ ). These differences are consistent with method-specific planimetric errors, which affect the inferred distance between adjacent transects and therefore slope estimation. For SfM, VGGT-Long, LiDAR, and VGGsFm, relative planimetric errors were 0.8%, 2.9%, 3.6%, and 4.4%, respectively. Because slope is often a dominant driver of flow in simplified hydraulic formulations, planimetric misalignment can strongly influence velocity estimates (Teng et al., 2017; Cohen et al., 2019).

For water depth, SfM reconstruction again produced the lowest error ( $\pm 10\%$ ). iPhone LiDAR reconstruction produced depth errors of  $-15\%$  to  $+25\%$ . VGGsFm and VGGT-Long reconstructions produced larger and broader depth errors (VGGsFm:  $-50\%$  to  $+10\%$ ; VGGT-Long:  $-10\%$  to  $+40\%$ ). These patterns align with prior work indicating that cross-sectional shape exerts strong control on depth estimation (Horritt and Bates, 2002; Pappenberger et al., 2005). Although depth and velocity are coupled for flow estimation (Manning, 1891; Gioia and Bombardelli, 2001), the results suggest that VGGT-Long's relatively better slope estimation (compared with VGGsFm) improved velocity predictions, but its poorer cross-sectional fidelity degraded depth estimates, bringing errors on depth estimation closer to those of VGGsFm reconstruction.

Nitrate uptake velocity is a function of flow velocity and depth, as introduced in Section 2.3. The relative error distributions for the nitrate uptake velocity, as shown in Figure 6c, are very similar to the relative error distributions for the velocity (Figure 6b). This is consistent with Equations 2, 3, where nitrate uptake velocity is proportional to the flow velocity but depends only weakly on water depth. This is also mentioned in Chen et al. (2024a), who noted that the relative error of nitrate uptake velocity is on the same order of magnitude as error of flow velocity.

Similarly, the reaeration rate constant is also a function of flow velocity and depth, but with stronger sensitivity to water depth (Owens et al., 1964). Therefore, the relative errors in depth estimation were amplified in reaeration rate constant estimates (Figure 6d). This explains why VGGsFm reconstruction, which is slightly worse than VGGT-Long reconstruction for depth, showed disproportionately larger reaeration rate constant errors. For this non-perennial stream, because reaeration formulations are usually inversely proportional to water depth (Al-Saadi and Al-Zubaidi, 2025), shallow streams' reaeration rate constant is especially sensitive to depth bias (Al-Saadi and Al-Zubaidi, 2025; Thys et al., 1987; Arora and Keshari, 2021).

### 4.4 Implications for future research

Future work should extend the error-propagation analysis beyond the simplified hydraulic formulations used here by coupling reconstructed topography to 2D or 3D numerical flow simulations (e.g., depth-averaged (Perkins and Richmond, 2004; Coon et al., 2020) or fully 3D multi-phase models (Bao et al., 2024; Chen et al., 2024b)). Such models would allow a more rigorous assessment of how spatially structured elevation and planimetric

errors influence flow fields, wetted extent, shear stress, and transport. This would help identify which components of reconstruction error most strongly control uncertainty in hydrobiogeochemical metrics under different discharge and channel-complexity conditions.

Finally, even the higher-error reconstructions evaluated here may still represent an improvement over relying solely on coarse resolution (1–10 m) DEM products, which often fail to resolve small non-perennial channels and low-flow pathways, limiting the feasibility of estimating reach-scale metabolism in these systems (Cavallo et al., 2022; Cavallo et al., 2025; USGS, 2024). As a result, low-cost reconstructions, particularly SfM when low-altitude imaging is feasible, may substantially expand the feasibility of reach-scale metabolism and transport analyses in non-perennial stream networks.

## 5 Conclusion

Without relying on RTK/PPK positioning or calibrations with GCPs, the standard SfM workflow using UAV imagery provided the most accurate and practically useful reconstruction of dry stream riverbeds among the methods tested, with propagated errors in hydrobiogeochemical estimates that are likely acceptable for many applications in non-perennial streams. In contrast, the learning-based reconstructions (VGGsFm and VGGT-Long), while substantially faster computationally, did not achieve sufficient geometric accuracy for small, shallow channels and produced large errors in derived hydraulic and biogeochemical metrics. These approaches are therefore not currently recommended for this setting unless accuracy can be improved through retraining or fine-tuning on imagery representative of natural stream corridors. iPhone LiDAR reconstructions were also inadequate for long stream reaches due to positional drift accumulated during scanning. While not preferred over SfM, if there are strong constraints such as limited computational power or UAV limitations, VGGT-Long may be useful for some hydrobiogeochemical parameter estimations and iPhone LiDAR may be useful for short segments for which UAV surveys are not possible.

## Data availability statement

The dataset presented in this study can be found in online repositories (Bao et al., 2025).

## Author contributions

JB: Formal Analysis, Software, Writing – review and editing, Data curation, Methodology, Writing – original draft, Visualization, Conceptualization, Validation. YC: Writing – review and editing, Conceptualization, Methodology. VG-C: Methodology, Writing – review and editing, Supervision, Data curation. EF-C: Writing – review and editing, Data curation, Methodology. ML: Methodology, Data curation, Writing – review and editing. JS:

Writing – review and editing, Data curation. KM: Data curation, Writing – review and editing. LR: Data curation, Writing – review and editing. BF: Data curation, Writing – review and editing. AG: Writing – review and editing, Data curation, Project administration. JS: Resources, Writing – review and editing, Funding acquisition, Conceptualization, Supervision.

## Funding

The author(s) declared that financial support was received for this work and/or its publication. This research was supported by the U.S. Department of Energy, Office of Science, Office of Biological and Environmental Research, Environmental System Science (ESS) Program. This contribution originates from the River Corridor Scientific Focus Area (SFA) project at Pacific Northwest National Laboratory (PNNL). Pacific Northwest National Laboratory is operated by Battelle Memorial Institute for the U.S. Department of Energy under Contract DE-AC05-76RL01830.

## Acknowledgements

We thank the Confederated Tribes and Bands of the Yakama Nation Tribal Council and Yakama Nation Fisheries for working with us to facilitate sample collection and optimization of data usage according to their values and worldview.

## Conflict of interest

The author(s) declared that this work was conducted in the absence of any commercial or financial relationships that could be construed as a potential conflict of interest.

## Generative AI statement

The author(s) declared that generative AI was not used in the creation of this manuscript.

Any alternative text (alt text) provided alongside figures in this article has been generated by Frontiers with the support of artificial intelligence and reasonable efforts have been made to ensure accuracy, including review by the authors wherever possible. If you identify any issues, please contact us.

## Publisher's note

All claims expressed in this article are solely those of the authors and do not necessarily represent those of their affiliated organizations, or those of the publisher, the editors and the reviewers. Any product that may be evaluated in this article, or claim that may be made by its manufacturer, is not guaranteed or endorsed by the publisher.

## References

- Al-Saadi, B. J. M., and Al-Zubaidi, H. A. M. (2025). Reaeration coefficient empirical equation selection for water quality modeling in surface waterbodies: an integrated numerical-modeling-based technique with field case study. *Limnol. Rev.* 25 (2), 15. doi:10.3390/limnolrev25020015
- Apple (2024). ARKit: integrate hardware sensing features to produce augmented reality apps and games. Available online at: <https://developer.apple.com/documentation/arkit> (Accessed January 05, 2026).
- Appling, A. P., Read, J. S., Winslow, L. A., Arroita, M., Bernhardt, E. S., Griffiths, N. A., et al. (2018). The metabolic regimes of 356 Rivers in the United States. *Sci. Data* 5, 180292. doi:10.1038/sdata.2018.292
- Arora, S., and Keshari, A. K. (2021). Modelling re-aeration of Rivers using predictive models and developed ANN models under varying hydrodynamic conditions. *Hydrological Sci. J.* 67 (15), 2294–2309. doi:10.1080/02626667.2022.2138402
- Bao, J., Song, X., Chen, Y., Fang, Y., Lin, X., Hou, Z., et al. (2024). On the transferability of residence time distributions in two 10-km long river sections with similar hydromorphic units. *J. Hydrology* 640, 131723. doi:10.1016/j.jhydrol.2024.131723
- Bao, J., Chen, Y., Garayburu-Caruso, V., Fluet-Chouinard, E., Laan, M., Smart, J., et al. (2025). Remote sensing images, DEM, and point clouds associated with “Accuracy Evaluation of Cost-Effective 3D Reconstruction Approaches for Non-Perennial Stream Riverbeds”. Available online at: <https://data.ess-dive.lbl.gov/view/> (Accessed December 15, 2025).
- Benjankar, R. M., Tonina, D., McKean, J. A., Sohrabi, M. M., Chen, Q., and Videgar, D. (2018). Dam operations May improve aquatic habitat and offset negative effects of climate change. *J. Environ. Manag.* 213, 126–134. doi:10.1016/j.jenvman.2018.02.066
- Bernhardt, E. S., Heffernan, J. B., Grimm, N. B., Stanley, E. H., Harvey, J. W., Arroita, M., et al. (2018). The metabolic regimes of flowing waters. *Limnol. Oceanogr.* 63, S99–S118. doi:10.1002/lno.10726
- Carbonneau, P. E., and Dietrich, J. T. (2017). Cost-effective non-metric photogrammetry from consumer-grade sUAS: implications for direct georeferencing of structure from motion photogrammetry. *Earth Surf. Process. Landforms* 42 (3), 473–486. doi:10.1002/esp.4012
- Cavallo, C., Papa, M. N., Negro, G., Gargiulo, M., Ruello, G., and Veza, P. (2022). Exploiting Sentinel-2 dataset to assess flow intermittency in non-perennial Rivers. *Sci. Rep.* 12, 21756. doi:10.1038/s41598-022-26034-z
- Cavallo, C., Sarno, L., Papa, M. N., Negro, G., Veza, P., Ruello, G., et al. (2025). Estimating dry bed periods in non-perennial Rivers using Sentinel-2 satellite data. *J. Hydrology* 660, 133416. doi:10.1016/j.jhydrol.2025.133416
- Chen, Y., Bao, J., Chen, R., Li, B., Yang, Y., Renteria, L., et al. (2024a). Quantifying streambed grain size, uncertainty, and hydrobiogeochemical parameters using machine learning model YOLO. *Water Resour. Res.* 60, e2023WR036456. doi:10.1029/2023WR036456
- Chen, Y., Bao, J., Fang, Y., Perkins, W. A., Ren, H., Song, X., et al. (2024b). Modeling of streamflow in a 30 km long reach spanning 5 years using OpenFOAM 5.x. *Geosci. Model Dev.* 15, 2917–2947. doi:10.5194/gmd-15-2917-2022
- Chen, Y., Liu, X., Zhu, B., Zhu, D., Zuo, X., and Li, Q. (2025). UAV image-based 3D reconstruction technology in landslide disasters: a review. *Remote Sensing* 17 (17), 3117. doi:10.3390/rs17173117
- Clapuyt, F., Vanacker, V., Schlunegger, F., and Oost, K. V. (2017). Unravelling Earth flow dynamics with 3-D time series derived from UAV-SfM models. *Earth Surf. Dyn.* 5, 791–806. doi:10.5194/esurf-5-791-2017
- Cohen, S., Raney, A., Munasinghe, D., Loftis, J. D., Molthan, A., Bell, J., et al. (2019). The floodwater depth estimation tool (FwDET v2.0) for improved remote sensing analysis of coastal flooding. *Nat. Hazards Earth Syst. Sci.* 19, 2053–2065. doi:10.5194/nhess-19-2053-2019
- Comport, A. I., Malis, E., and Rives, P. (2010). Real-time quadrifocal visual odometry. *Int. J. Robotics Res.* 29 (3), 245–266. doi:10.1177/02783649093356
- Cook, A., and Merwade, V. (2009). Effect of topographic data, geometric configuration and modeling approach on flood inundation mapping. *J. Hydrology* 377 (1–2), 131–142. doi:10.1016/j.jhydrol.2009.08.015
- Coon, E. T., Moulton, J. D., Kikinzon, E., Berndt, M., Manzini, G., Garimella, R., et al. (2020). Coupling surface flow and subsurface flow in complex soil structures using mimetic finite differences. *Adv. Water Resour.* 144, 103701. doi:10.1016/j.advwatres.2020.103701
- Dai, W., Qiu, R., Wang, B., Lu, W., Zheng, G., Amankwah, S. O. Y., et al. (2023). Enhancing UAV-SfM photogrammetry for terrain modeling from the perspective of spatial structure of errors. *Remote Sensing* 15 (17), 4305. doi:10.3390/rs15174305
- Datry, T., Larned, S. T., and Tockner, K. (2014). Intermittent Rivers: a challenge for freshwater ecology. *BioScience* 64 (3), 229–235. doi:10.1093/biosci/bit027
- Deng, K., Ti, Z., Xu, J., Yang, J., and Xie, J. (2025). VGGT-Long: chunk it, loop it, align it – pushing vggT’s limits on kilometer-scale long RGB sequences. *arXiv*. arXiv:2507.16443v1.
- Dietrich, J. T. (2016). Riverscape mapping with helicopter-based structure-from-motion photogrammetry. *Geomorphology* 252, 144–157. doi:10.1016/j.geomorph.2015.05.008
- Dietrich, J. T. (2017). Bathymetric Structure-from-Motion: extracting shallow stream bathymetry from multi-view stereo photogrammetry. *Earth Surf. Process. Landforms* 42 (2), 243–386. doi:10.1002/esp.4060
- DJI Matrice 300 RTK user manual (2025). DJI Matrice 300 RTK user manual. Available online at: <https://www.dji.com/downloads/products/matrice-300#doc> (Accessed January 06, 2026).
- Dosovitskiy, A. (2024). *An image is worth 16x16 words: transformers for image recognition at scale*. arXiv:2010.11929v2.
- Elias, M., Isfort, S., Eltner, A., and Maas, H. (2024). “UASPhotogrammetry for precise digital elevation models of complex topography: a strategy guide,” in *Presented at the SPRS TC II mid-term symposium “the role of photogrammetry for a sustainable world*. Nevada, USA: Las Vegas.
- Eltner, A., Kaiser, A., Castillo, C., Rock, G., Neugirg, F., and Abellan, A. (2016). Image-based surface reconstruction in geomorphometry – merits, limits and developments. *Earth Surf. Dyn.* 4, 359–389. doi:10.5194/esurf-4-359-2016
- Entwistle, N., Heritage, G., and Milan, D. (2018). Recent remote sensing applications for hydro and morphodynamic monitoring and modelling. *Earth Surf. Process. Landforms* 43 (10), 2283–2291. doi:10.1002/esp.4378
- Ferguson, R. (2007). Flow resistance equations for gravel- and boulder-bed streams. *Water Resour. Res.* 43 (5), W05427. doi:10.1029/2006WR005422
- Ferguson, R. (2022). Reach-scale flow resistance. *Treatise Geomorphol.* 6 (1), 110–132. doi:10.1016/B978-0-12-409548-9.09386-6
- Flener, C., Vaaja, M., Jaakkola, A., Krooks, A., Kaartinen, H., Kukko, A., et al. (2013). Seamless mapping of river channels at high resolution using Mobile LiDAR and UAV-photography. *Remote Sensing* 5 (12), 6382–6407. doi:10.3390/rs5126382
- Fonstad, M. A., Dietrich, J. T., Courville, B. C., Jensen, J. L., and Carbonneau, P. E. (2013). Topographic structure from motion: a new development in photogrammetric measurement. *Earth Surf. Process. Landforms* 38 (4), 421–430. doi:10.1002/esp.3366
- Frankl, A., Stal, C., Abraha, A., Nysen, J., Rieke-Zapp, D., De Wulf, A., et al. (2015). Detailed recording of gully morphology in 3D through image-based modelling. *CATENA* 127, 92–101. doi:10.1016/j.catena.2014.12.016
- Gaidon, A., Wang, Q., Cabon, Y., and Vig, E. (2016). “Virtual worlds as proxy for multi-object tracking analysis,” in *Presented at the 2016 IEEE conference on computer vision and pattern recognition (CVPR)*, Las Vegas, NV, USA.
- Geiger, A., Lenz, P., and Urtasun, R. (2012). “Are we ready for autonomous driving? The KITTI vision benchmark suite,” in *Presented at the 2012 IEEE conference on computer vision and pattern recognition*. Providence, RI, USA.
- Gellenbeck, K. (1999). “A spatial and temporal analysis of riparian vegetation along satus creek on the yakama Indian reservation,” in *Master, resource management*. Central Washington University, Central Washington University. Available online at: <https://digitalcommons.cwu.edu/etd/1786> (Accessed September 10, 2025).
- Gioia, G., and Bombardelli, F. A. (2001). Scaling and similarity in rough channel flows. *Phys. Rev. Lett.* 88, 014501. doi:10.1103/PhysRevLett.88.014501
- Giulietti, N., Allevi, G., Castellini, P., Garinei, A., and Martarelli, M. (2022). Rivers’ water level assessment using UAV photogrammetry and RANSAC method and the analysis of sensitivity to uncertainty sources. *Sensors* 22 (14), 5319. doi:10.3390/s22145319
- Gollob, C., Ritter, T., Krabnitzer, R., Tockner, A., and Nothdurft, A. (2021). Measurement of forest inventory parameters with apple iPad pro and integrated LiDAR technology. *Remote Sens.* 13 (16), 3129. doi:10.3390/rs13163129
- Gonzalez, R., and Woods, R. (2017). *Digital image processing*. 4th ed. Boston, MA: Pearson.
- Grant, S. B., Azizian, M., Cook, P., Boano, F., and Rippy, M. A. (2018). Factoring stream turbulence into global assessments of nitrogen pollution. *Science* 359 (6381), 1266–1269. doi:10.1126/science.aap8074
- Grieger, S. (2014). *Spatial study 2021: sample-based surface water chemistry and organic matter characterization across watersheds in the yakima river basin*. Washington, USA. doi:10.15485/1898914
- Guide to optical levels (2023). Guide to optical levels. Available online at: <https://uk.rs-online.com/web/content/discovery/ideas-and-advice/optical-levels-guide> (Accessed September 10, 2025).
- Hardy, R. J., Bates, P. D., and Anderson, M. G. (1999). The importance of spatial resolution in hydraulic models for floodplain environments. *J. Hydrology* 216, 124–136. doi:10.1016/S0022-1694(99)00002-5
- Harley, A. W., Fang, Z., and Fragkiadaki, K. (2022). Particle video revisited: tracking through occlusions using point trajectories. *arXiv*. arXiv:2204.04153v2.
- Hartley, R., and Zisserman, A. (2000). *Multiple view geometry in computer vision. The Edinburgh building*. Cambridge cb2 2ru. UK: Cambridge University Press.
- Harvey, J. W., Choi, J., and Quion, K. (2024). Metabolism regimes in regulated Rivers of the illinois river basin, USA. *Sci. Data* 11 (211), 211. doi:10.1038/s41597-024-03037-1
- He, X. (2024). *Detector-free structure from motion*. arXiv:2306.15669v1.

He, K., Zhang, X., Ren, S., and Sun, J. (2016). "Deep residual learning for image recognition," in *Presented at the 2016 IEEE conference on computer vision and pattern recognition (CVPR), Las Vegas, NV, USA*.

Horritt, M. S., and Bates, P. D. (2002). Evaluation of 1D and 2D numerical models for predicting river flood inundation. *J. Hydrology* 268 (1-4), 87–99. doi:10.1016/S0022-1694(02)00121-X

Huai, J., Shao, Y., and Zhang, Y. (2025). A low-cost portable lidar-based Mobile mapping system on an android smartphone. *arXiv*. arXiv:2506.15983v1.

IPTC (2025). Exif 3.0 released, featuring UTF-8 support. Available online at: <https://iptc.org/news/exif-3-0-released-features-utf-8-support/> (Accessed September 10, 2025).

Jaulin, L. (2011). Range-only SLAM with occupancy maps: A set-membership approach. *IEEE Trans. Robotics* 27 (5), 1004–1010. doi:10.1109/TRO.2011.2147110

Javernick, L., Brasington, J., and Caruso, B. (2014). Modeling the topography of shallow braided Rivers using structure-from-motion photogrammetry. *Geomorphology* 213, 166–182. doi:10.1016/j.geomorph.2014.01.006

Karaev, N., Rocco, I., Graham, B., Neverova, N., Vedaldi, A., and Rupprecht, C. (2023). CoTracker: it is better to track together. *arXiv*. arXiv:2307.07635v3.

Keim, R. F., Skaugset, A. E., and Bateman, D. S. (1999). Digital terrain modeling of small stream channels with a total-station theodolite. *Adv. Water Resour.* 23 (1), 41–48. doi:10.1016/S0309-1708(99)00007-X

King, D. (2024). Beginners guide for optical levels. Available online at: <https://learnframing.com/setting-up-optical-level-transit/> (Accessed September 10, 2025).

Krauskova, D., Mikita, T., Hruza, P., and Kudrnova, B. (2025). Accuracy assessment of iPhone LiDAR for mapping streambeds and small water structures in forested terrain. *Sensors* 25 (19), 6141. doi:10.3390/s25196141

Kurz, M. J., Drummond, J. D., Martí, E., Zarnetske, J. P., Lee-Cullin, J., Klaar, M. J., et al. (2017). Impacts of water level on metabolism and transient storage in vegetated lowland Rivers: insights from a mesocosm study. *J. Geophys. Res. Biogeosciences* 122, 628–644. doi:10.1002/2016JG003695

Lague, D. (2020). Chapter 8 - terrestrial laser scanner applied to fluvial geomorphology. *Dev. Earth Surf. Process.* 23, 231–254. doi:10.1016/B978-0-444-64177-9.00008-4

Lamsters, K., Jeskins, J., Sobota, I., Karuss, J., and Dzerins, P. (2022). Surface characteristics, elevation change, and velocity of high-arctic valley glacier from repeated high-resolution UAV photogrammetry. *Remote Sens.* 14 (4), 1029. doi:10.3390/rs14041029

Larned, S. T., Datry, T., Arscott, D. B., and Tockner, K. (2010). Emerging concepts in temporary-river ecology. *Freshw. Biol.* 55, 717–738. doi:10.1111/j.1365-2427.2009.02322.x

Legleiter, C. J., and Harrison, L. R. (2018). Remote sensing of river bathymetry: evaluating a range of sensors, platforms, and algorithms on the upper sacramento river, California, USA. *Water Resour. Res.* 55 (3), 2142–2169. doi:10.1029/2018WR023586

Li, Z., and Snavely, N. (2018). "MegaDepth: learning single-view depth prediction from internet photos." *arXiv:1804.00607v4*. arXiv

Li, M., Giorgio, P., Parkes, A. H., and Prairie, Y. T. (2015). The relative influence of topography and land cover on inorganic and organic carbon exports from catchments in southern Quebec, Canada. *JGR Biogeosciences* 120 (12), 2562–2578. doi:10.1002/2015JG003073

Li, Y., Huang, S., Chen, Y., Ding, Y., Zhao, P., Hu, Q., et al. (2024). RGBTSDf: an efficient and simple method for color truncated signed distance field (TSDF) volume fusion based on RGB-D images. *Remote Sens.* 16 (17), 3188. doi:10.3390/rs16173188

Liang, X., Hyyppä, J., Kaartinen, H., Lehtomäki, M., Pyörälä, J., Pfeifer, N., Yu, X., et al. (2018a). International benchmarking of terrestrial laser scanning approaches for forest inventories. *ISPRS J. Photogrammetry Remote Sens.* 144, 137–179. doi:10.1016/j.isprsjprs.2018.06.021

Liang, X., Kukko, A., Hyyppä, J., Lehtomäki, M., Pyörälä, J., et al. (2018b). *In-situ* measurements from Mobile platforms: an emerging approach to address the old challenges associated with forest inventories. *ISPRS J. Photogrammetry Remote Sens.* 143, 97–107. doi:10.1016/j.isprsjprs.2018.04.019

Lin, A., Zhang, J. Y., Ramanan, D., and Tulsiani, S. (2024). *RelPose++: recovering 6D poses from sparse-view observations*. arXiv:2305.04926v2.

Lindenberger, P., Sarlin, P. E., Larsson, V., and Pollefeys, M. (2021). Pixel-perfect structure-from-motion with featuremetric refinement. *arXiv*. arXiv:2108.08291v1.

Liu, L. (2023). Drone-based photogrammetry for riverbed characteristics extraction and flood discharge modeling in taiwan's mountainous Rivers. *Measurement* 220, 113386. doi:10.1016/j.measurement.2023.113386

Lorensen, W. E., and Cline, H. E. (1987). Marching cubes: a high resolution 3D surface construction algorithm. *ACM SIGGRAPH Comput. Graph.* 21 (4), 163–169. doi:10.1145/37402.3742

Lourakis, M. I. A., and Argyros, A. A. (2009). SBA: a software package for generic sparse bundle adjustment. *ACM Trans. Math. Softw.* 36 (1), 1–30. doi:10.1145/1486525.1486527

Lowe, D. G. (1999). Object recognition from local scale-invariant features. *Seventh IEEE Int. Conf. on Comput. Vis. Kerkyra, Greece* 2, 1150–1157. doi:10.1109/ICCV.1999.790410

Luetzenburg, G., Kroon, A., and Bjork, A. A. (2021). Evaluation of the apple iPhone 12 pro LiDAR for an application in geosciences. *Sci. Rep.* 11, 22221. doi:10.1038/s41598-021-01763-9

Magnabosco, M., and Breckon, T. P. (2013). Cross-spectral visual simultaneous localization and mapping (SLAM) with sensor handover. *Robotics Aut. Syst.* 61 (2), 195–208. doi:10.1016/j.robot.2012.09.023

Manning, R. (1891). On the flow of water in open channels and pipes. *Trans. Institution Civ. Eng. Ire.* 20, 161–207.

Medeiros, B., Candido, B., Jimenez, P. A. J., Avanzi, J. C., and Silva, M. L. N. (2025). UAV-based soil water erosion monitoring: current status and trends. *Drones* 9 (4), 305. doi:10.3390/drones9040305

Mokros, M., Mikita, T., Singh, A., Tomaštk, J., Chudá, J., Weżyk, P., et al. (2021). Novel low-cost Mobile mapping systems for forest inventories as terrestrial laser scanning alternatives. *Int. J. Appl. Earth Observation Geoinformation* 104, 102512. doi:10.1016/j.jag.2021.102512

Moudrý, V., Gdulová, K., Fogl, M., Klápště, P., Urban, R., Komárek, J., et al. (2019). Comparison of leaf-off and leaf-on combined UAV imagery and airborne LiDAR for assessment of a post-mining site terrain and vegetation structure: prospects for monitoring hazards and restoration success. *Appl. Geogr.* 104, 32–41. doi:10.1016/j.apgeog.2019.02.002

Mulholland, P. J., Fellows, C. S., Tank, J. L., Grimm, N. B., Webster, J. R., Hamilton, S. K., et al. (2008). Inter-biome comparison of factors controlling stream metabolism. *Freshw. Biol.* 46, 1503–1517. doi:10.1046/j.1365-2427.2001.00773.x

Mundorff, M. J., Nish, R. D. M., and Cline, D. R. (1977). *Water resources of the satus creek basin*. Washington: Yakima Indian Reservation.

NOAA (2025). GPS accuracy. Available online at: <https://www.gps.gov/systems/gps/performance/accuracy/> (Accessed September 10, 2025).

Novais, J., Vieira, A., Bento-Goncalves, A., Silva, S., Folharini, S., and Marques, T. (2023). The use of UAVs for morphological coastal change monitoring—A bibliometric analysis. *Drones* 7 (10), 629. doi:10.3390/drones7100629

Oikawa, N., Nakagawa, Y., Owari, T., Tatsumi, S., and Suzuki, S. N. (2025). Utilising LiDAR-equipped iPhone in forestry: constructing 3D models and measuring tree sizes in a planting site. *Ecol. Solutions Evid.* 6 (1), e12399. doi:10.1002/2688-8319.12399

Open Drone Map (2025). ODM - a command line toolkit to generate maps, point clouds, 3D models and DEMs from drone, balloon or kite images. Available online at: <https://github.com/OpenDroneMap/ODM> (Accessed September 10, 2025).

Owens, M., Edwards, R. W., and Gibbs, J. W. (1964). Some reaeration studies in streams. *Int. J. Air Water Pollut.* 8, 469–486.

Pappenberger, F., Beven, K., Horritt, M., and Blazkova, S. (2005). Uncertainty in the calibration of effective roughness parameters in HEC-RAS using inundation and downstream level observations. *J. Hydrology* 302 (1-4), 46–69. doi:10.1016/j.jhydrol.2004.06.036

Perera, S., Barnes, N., He, X., Izadi, S., Kohli, P., and Glocker, B. (2015). "Motion segmentation of truncated signed distance function based volumetric surfaces," in *Presented at the 2015 IEEE winter conference on applications of computer vision, waikoloa, HI, USA*.

Perkins, W., and Richmond, M. (2004). *MASS2, modular aquatic simulation system in two dimensions, user guide and reference*.

Picioreanu, C., Loosdrecht, M. C., and Heijnen, J. J. (1997). Modelling the effect of oxygen concentration on nitrite accumulation in biofilm airlift suspension reactor. *Water Sci. Technol.* 36 (1), 147–156. doi:10.2166/wst.1997.0034

Pineda, L., Fan, T., Monge, M., Venkataraman, S., Sodhi, P., Chen, R.T.Q., et al. (2023). *Theseus: a library for differentiable nonlinear optimization*. arXiv:2207.09442v3.

Polycam (2023). Polycam 3D scanner, LiDAR. Available online at: <https://polycam.com/> (Accessed September 10, 2025).

Rosas, M. A., Clapuyt, F., Viveen, W., and Vanacker, V. (2023). Quantifying geomorphic change in andean river valleys using UAV-PPK-SfM techniques: an example from the Western Peruvian andes. *Geomorphology* 435, 108766. doi:10.1016/j.geomorph.2023.108766

Scaniverse (2023). "Scaniverse," in *Scaniverse*. Available online at: <https://scaniverse.com/> (Accessed January 05, 2026).

Schaffalitzky, F., and Zisserman, A. (2002). Multi-view matching for unordered image sets, or how do I organize my holiday snaps?, in *Eccv '02: proceedings of the 7th European conference on computer vision-part I*, 414–443. doi:10.1007/3-540-47969-4\_28

Schönberger, J. L., and Frahm, J. M. (2016). "Structure-from-Motion revisited," in *Presented at the CVPR*.

Sestras, P., Badea, G., Badea, A. C., Salagean, T., Oniga, V. E., Roșca, S., et al. (2025). A novel method for landslide deformation monitoring by fusing UAV photogrammetry and LiDAR data based on each sensor's mapping advantage in regards to terrain feature. *Eng. Geol.* 346, 107890. doi:10.1016/j.enggeo.2024.107890

- Shan, J., and Toth, C. K. (2018). *Topographic laser ranging and scanning, principles and processing*. Boca Ration, FL: CRC Press.
- Shogren, A. J., Zarnetske, J. P., Abbott, B. W., Iannucci, F., Frei, R. J., Griffin, N. A., et al. (2019). Revealing biogeochemical signatures of arctic landscapes with river chemistry. *Sci. Rep.* 9 (1), 12894. doi:10.1038/s41598-019-49296-6
- SiteScape (2024). *SiteScape*. Available online at: <https://www.sitescape.ai/> (Accessed January 05, 2026).
- Skydio (2024). *Comparing skydio 2 and skydio 2+*. Available online at: <https://support.skydio.com/hc/en-us/articles/5338292379803-Comparing-Skydio-2-and-Skydio-2> (Accessed September 10, 2025).
- Sledz, S., Ewertowski, M. W., and Piekarczyk, J. (2021). Applications of unmanned aerial vehicle (UAV) surveys and structure from motion photogrammetry in glacial and periglacial geomorphology. *Geomorphology* 378, 107620. doi:10.1016/j.geomorph.2021.107620
- Snelder, T. H., Datz, T., Lamouroux, N., Larned, S. T., Sauquet, E., Pella, H., et al. (2013). Regionalization of patterns of flow intermittence from gauging station records. *Hydrol. Earth Syst. Sci.* 17 (7), 2685–2699. doi:10.5194/hess-17-2685-2013
- SRL (2024). 3d scanner app. Available online at: <https://apps.apple.com/us/app/3d-scanner-app/id1419913995> (Accessed September 10, 2025).
- Stegen, J., Burgin, A., Busch, M., Fisher, J., Ladau, J., Abrahamson, J., et al. (2024). *Reviews and syntheses: variable inundation across earth's terrestrial ecosystems*. EGUsphere Preprint. doi:10.5194/egusphere-2024-98
- Sun, P., Kretschmar, H., Dotiwala, X., Chouard, A., Patnaik, V., Tsui, P., et al. (2020). "Scalability in perception for autonomous driving: waymo open dataset," in *Presented at the 2020 IEEE/CVF conference on computer vision and pattern recognition (CVPR)*. Seattle, WA, USA.
- Tang, C., and Tan, P. (2018). *Ba-net: dense bundle adjustment network*. arXiv:1806.04807.
- Tatsumi, S., Yamaguchi, K., and Furuya, N. (2022). ForestScanner: a Mobile application for measuring and mapping trees with LiDAR-equipped iPhone and iPad. *Methods Ecol. Evol.* 14 (7), 1603–1609. doi:10.1111/2041-210X.13900
- Teed, Z., and Deng, J. (2018). Deepv2d: video to depth with differentiable structure from motion. *arXiv*. arXiv:1812.04605.
- Teed, Z., and Deng, J. (2021). Droid-slam: deep visual slam for monocular, stereo, and rgb-d cameras. *arXiv*. doi:10.48550/arXiv.2108.10869
- Teng, J., Jakeman, A. J., Vaze, J., Croke, B. F. W., Dutta, D., and Kim, S. (2017). Flood inundation modelling: a review of methods, recent advances and uncertainty analysis. *Environ. Model. and Softw.* 90, 201–216. doi:10.1016/j.envsoft.2017.01.006
- Thyssen, N., and Erlandsen, M. (1987). Reaeration of oxygen in shallow, macrophyte rich streams: II. Relationship between the reaeration rate coefficient and hydraulic properties. *Hydrobiologia* 72 (5), 575–597. doi:10.1002/iroh.19870720505
- Triggs, B., McLauchlan, P., Hartley, R., and Fitzgibbon, A. (1999). "Bundle adjustment – a modern synthesis," in *International workshop on vision algorithms* (Springer-Verlag), 298–372. doi:10.1007/3-540-44480-7\_21
- Tromboni, F., Hotchkiss, E. R., Schechner, A. E., Dodds, W. K., Poulson, S. R., and Chandra, S. (2022). High rates of daytime river metabolism are an underestimated component of carbon cycling. *Commun. Earth and Environ.* 3, 270. doi:10.1038/s43247-022-00607-2
- Ullman, S. (1979). The interpretation of structure from motion. *Proc. R. Soc. B* 203 (1153), 405–426. doi:10.1098/rspb.1979.0006
- USGS (2024). 1 meter digital elevation models (DEMs) – USGS national map 3DEP downloadable data. Available online at: <https://data.usgs.gov/datacatalog/data/USGS:77ae0551-c61e-4979-aedd-d797abcdcde0e#:~:text=The%20DEM%20is%20produced%20from%20high%20resolution,images%20All%203DEP%20products%20are%20public%20domain> (Accessed September 10, 2025).
- Vaswani, A., Shazeer, N., Parmar, N., Uszkoreit, J., Jones, L., Gomez, A. N., et al. (2017). Attention is all you need. *arXiv*. arXiv:1706.03762v7.
- Wang, J., Chen, M., Karaev, N., Vedaldi, A., Ruppert, C., and Novotny, D. (2022). *VGIT: visual geometry grounded transformer*. arXiv:2503.11651v1.
- Wang, J., Karaev, N., Ruppert, C., and Novotny, D. (2023). *Visual geometry grounded deep structure from motion*. arXiv:2312.04563v1.
- Wang, J., Ruppert, C., and Novotny, D. (2024). PoseDiffusion: solving pose estimation via diffusion-aided bundle adjustment. *arXiv*. arXiv:2306.15667v4.
- Wang, Q., Fang, N., Zeng, Y., Yuan, C., Dai, W., Fan, R., et al. (2025). Optimizing UAV-SfM photogrammetry for efficient monitoring of gully erosion in high-relief terrains. *Measurement* 256, 118154. doi:10.1016/j.measurement.2025.118154
- Witek, M., Walusiak, G., Halicki, M., Remisz, J., Borowicz, D., Parzóch, K., et al. (2025). Reconstructing bed topography of a shallow river from close-range aerial imagery: multi-UAV experimental campaign in the izera river (SW Poland/N Czechia). *Geomorphology* 471, 109544. doi:10.1016/j.geomorph.2024.109544
- Yavuz, M., and Tufekcioglu, M. (2023). Assessment of flood-induced geomorphic changes in sidere creek of the mountainous basin using small UAV-based imagery. *Sustainability* 15 (15), 11793. doi:10.3390/su151511793
- Young, R. G., and Huryn, A. D. (1999). Effects of land use on stream metabolism and organic matter turnover. *Ecol. Appl.* 9 (4), 1359–1376. doi:10.1890/1051-0761(1999)009[1359:EOLUOS]2.0.CO;2
- Zhang, J. Y., Ramanan, D., and Tulsiani, S. (2022). RelPose: predicting probabilistic relative rotation for single objects in the wild. *arXiv*. arXiv:2208.05963v2.